JACS
JOURNAL OF THE AMERICAN CHEMICAL SOCIETY

Communication

pubs.acs.org/JACS

Noncovalently Functionalized Monolayer Graphene for Sensitivity Enhancement of Surface Plasmon Resonance Immunosensors

Meenakshi Singh,[†,‡] Michael Holzinger,*[,†] Maryam Tabrizian,[‡] Sinéad Winters,[§] Nina C. Berner,[§] Serge Cosnier,*[,†] and Georg S. Duesberg[§]

[†]Département de Chimie Moléculaire, Univ. Grenoble Alpes, CNRS, UMR 5250, F-38000 Grenoble, France

[‡]Biomat'X Research Laboratories, Dept. of Biomedical Engineering and Faculty of Dentistry, McGill University, Montréal, Quebec H3A 0G4, Canada

[§]School of Chemistry, Centre for Research on Adaptive Nanostructures and Nanodevices (CRANN) and Advanced Materials Bio-Engineering Research Centre (AMBER), Trinity College, Dublin 2, Ireland

Supporting Information

ABSTRACT: A highly efficient surface plasmon resonance (SPR) immunosensor is described using a functionalized single graphene layer on a thin gold film. The aim of this approach was two-fold: first, to amplify the SPR signal by growing graphene through chemical vapor deposition and, second, to control the immobilization of biotinylated cholera toxin antigen on copper coordinated nitrilotriacetic acid (NTA) using graphene as an ultrathin layer. The NTA groups were attached to graphene via pyrene derivatives implying $\pi-\pi$ interactions. With this setup, an immunosensor for the specific antibody anticholera toxin with a detection limit of 4 pg mL^{-1} was obtained. In parallel, NTA polypyrrole films of different thicknesses were electrogenerated on the gold sensing platform where the optimal electropolymerization conditions were determined. For this optimized polypyrrole-NTA setup, the simple presence of a graphene layer between the gold and polymer film led to a significant increase of the SPR signal.

Surface plasmon resonance (SPR) is an established technique for the study of biomolecular interactions and the transduction of biological recognition events in real time without requiring supplemental labeling steps.[1] The principle of this technique is based on light stimulated oscillation of electrons in the conduction band of usually gold films, called resonant surface plasmons. This phenomenon is strongly dependent on the dielectric constant of its environment[2] and represents a great advantage for biosensing applications since a biological receptor−analyte interaction results in a change of the oscillation frequency which can be recorded by measuring the angle change, intensity, refractive index, or phase of the reflected light.[1,3]

Extensive efforts were invested to improve the sensitivity of SPR signals using, e.g., gold nanoparticles,[4] quantum dots,[5] or Au/Ag alloy nanocomposites.[6] In terms of targeted immobilization of bioreceptor units on gold surfaces for SPR biosensing, self-assembled (SAM) molecular monolayers[7] or electrogenerated functional polymers[8] are often used. As known, the SPR sensitivity strongly depends on the thickness and dielectric constant of such functional layers on the surface. Therefore, due to a one atom thick sheet of carbon atoms in a hexagonal lattice and the recent development of its large-scale synthesis and transfer techniques as well as its functionalization, graphene should be an excellent candidate for SPR signal enhancement[9,10] and label-free monitoring of chemical or biomolecular interactions.[11,12] In addition to its high carrier mobility and zero-band gap characteristics, graphene also exhibits unique and desirable optical properties, such as broadband and tunable absorptions.[13,14] It has been shown that light transmittance through monolayer graphene is 97.7%,[15] e.g., a one-atom-thick graphene layer will absorb only 2.3% of incident light.

Theoretical models have predicted that the incorporation of a single layer of graphene can amplify significantly the optical sensitivity of SPR sensors.[16] The beneficial optical properties of graphene monolayers in the visible light range[17] lead to a change of the propagation constant of surface plasmon polariton (SPP), thus amplifying the change of the refractive index.[18]

Furthermore, biomolecules containing hydrophobic domains or π-systems like DNA strands or proteins tend to adsorb spontaneously on graphene.[19] Graphene can also easily be functionalized[20] and thus be modified for targeted immobilization of bioreceptor units.

Most of the reported graphene-based SPR biosensors utilize graphene oxide,[21] reduced graphene oxide,[22] or graphene decorated metal nanoparticles[23,24] as a sensing platform. However, the main limitation of this approach is the lack of homogeneous and defect-free monolayers on the SPR sensing platform, hindering the exploitation of the benefits of graphene.

Chemical vapor deposition (CVD) growth that can provide large scale monolayers of graphene with low defect densities is an attractive alternative method to the previously reported SPR substrates.[25] However, so far graphene monolayers for SPR biosensing have been mainly investigated numerically[26] and/or by using DNA[27] or protein adsorption[28] on the SPR chip surface.

This study reports on the beneficial optical properties of a single graphene sheet obtained by CVD for SPR biosensing applications. Graphene was modified for the controlled immobilization of the receptor unit, antigen cholera toxin either with a functional polypyrrole film or via noncovalent functionalization using pyrene derivatives[29] where the pyrene

Received: November 9, 2014

DOI: 10.1021/ja511512m
J. Am. Chem. Soc. XXXX, XXX, XXX−XXX

layer was reinforced by electropolymerization.[30,31] Both, the polypyrrole and the pyrene groups contain the anchoring nitrilotriacetic acid (NTA) group for the immobilization of the specific biotin tagged receptor, cholera toxin as illustrated in Figure 1.

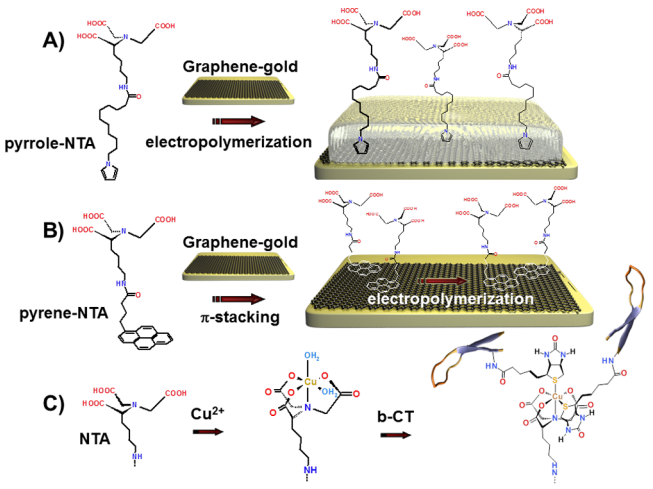

Figure 1. Schematic presentation of the functionalization of the graphene layer via (A) electropolymerization of a polypyrrole-NTA and (B) π stacking of pyrene-NTA followed by electropolymerization for the reinforcement of the layer. (C) Reaction scheme of the conditioning of the NTA group for the immobilization of b-CT.

The synthesis of graphene and its transfer to gold is described in the Supporting Information (SI). Great care was taken to supply homogeneous graphene with little defect density and polymer residues,[32,33] to supply a clean surface for further functionalization. Raman imaging is a very powerful tool to evaluate carbon surfaces.[34] In Figure 2 averaged Raman spectra

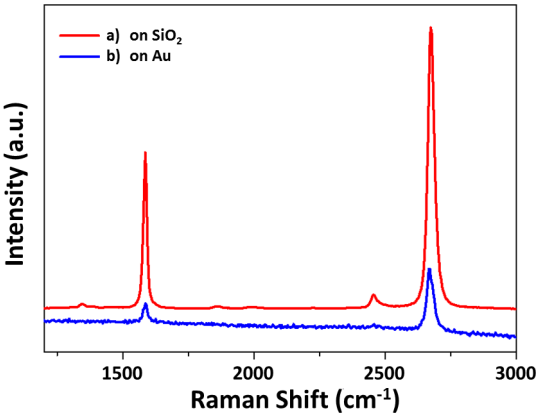

Figure 2. Average Raman spectra of pristine single layer graphene on (a) SiO_2 and (b) gold substrates.

of single-layer graphene, composed of 10,000 spectra taken over an area of 40 × 40 μm are shown. On SiO_2 substrate, D-, G-, and 2D peaks appear at 1350, 1583, and 2680 cm^{-1}, respectively using 532 nm excitation wavelength. The gold substrate spectrum is noisier and has a sloped background due to emission from the metal substrate (Figure 2b)[35,36] The intensity of the graphene peaks is enhanced on SiO_2 due to interference on the dielectric substrate,[37] which allows a detailed assessment of the graphene quality by Raman imaging shown in Figure S1. While the D band in combination with the D/G band ratio gives insight into the quality of graphene in terms of defects in the graphene's π-system, the 2D band is representative for the number of graphene layers.[38] The Raman spectra in Figure 2 clearly indicate the presence of high-quality monolayer graphene due to the almost negligible presence of a D band and the sharp and symmetric 2D band as well as the high 2D/G peak ratio.[39,40] Further Raman analysis, optical images and XPS spectra showing the continuity and high quality of the graphene are provided in Figures S1 and S3.

Effective immobilization of biomolecules on the sensor surface is one of the most challenging steps in the development of high-performance biosensors.[41] To secure this requirement, the NTA-Cu^{2+}/biotin system was used.[42] Furthermore, noncovalent functionalization using π-stacking interactions or electropolymerization was also an important consideration in order to preserve the properties of graphene.

A detailed procedure of the functionalization of the gold surface via electropolymerization of pyrrole-NTA as well as the electrochemical coating and noncovalent attachment of pyrene-NTA can be found in the SI. Three polymer films of different thicknesses were electrogenerated giving coatings of 5.66, 16.9, and 28.3 nmol·cm^{-2} for the electropolymerization conditions at 1, 3, and 5 mC·cm^{-2}, respectively. The resulting polypyrrole-NTA films thicknesses were estimated using a confocal laser microscope and gave around 100 nm for 1 mC·cm^{-2}, 270 nm for 3 mC·cm^{-2}, and 450 nm for 5 mC·cm^{-2}. These films were used for the successive attachment of the bioreceptor unit (biotinylated cholera toxin, b-CT) via subsequent coordination of copper(II) ions at the NTA chelate and b-CT.

The immunoreaction between the immobilized b-CT and the analyte, anticholera toxin from rabbit (anti-CT), was monitored in the angle shift mode in real time. The angle shift is correlated with the changing thickness and optical properties of the sensing layer. The response also depends on the refractive index of the bulk solution. There is a linear relationship between the amount of bound material (analyte) and the SPR angle shift.[43] These angle shifts are in the order of millidegrees (mdeg) and are used as a response unit to quantify the binding of the analyte to the sensor surface. Control experiments were performed without immobilization of the receptor antigen cholera toxin (Table S1), and all experiments were conducted three times to examine the reliability of the assays.

After demonstrating that the thinnest polymer film gives the highest SPR angle change (Figure S2), the conditions for the electropolymerization of such films of 100 nm thickness were applied to graphene-modified gold disks. Figure 3 shows the SPR angle change of polypyrrole-NTA/Cu^{2+}/b-CT on pure gold films and polypyrrole-NTA/Cu^{2+}/b-CT graphene-gold films for 35 and 4 ng·mL^{1} injection of anti-CT. The polypyrrole-NTA/Cu^{2+}/b-CT modified graphene-gold slides showed an angle change of 324 mdeg for 35 ng·mL^{-1} and 70 mdeg for 4 ng·mL^{-1} anti-CT, respectively, which is significantly higher than for the same configuration without the graphene monolayer (183 and 31 mdeg, respectively).

For these concentrations of analyte, the simple presence of a graphene monolayer led to an almost 2-fold increase of the angle shift. Such signal amplification was also observed for the reflectivity mode as summarized in Table S1. A 9% increase in reflectivity was recorded with graphene-based SPR immnosensor. For pure gold surfaces, the reflectivity change was 7%. A control experiment was performed with gold polypyrrole-NTA/Cu^{2+} and graphene-gold polypyrrole-NTA/Cu^{2+} in absence of

DOI: 10.1021/ja511512m
J. Am. Chem. Soc. XXXX, XXX, XXX−XXX

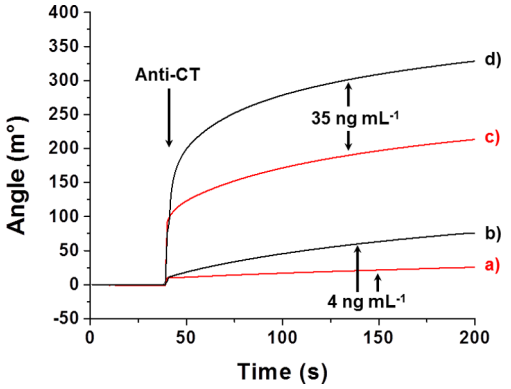

Figure 3. SPR angle shift after anti-CT injection using pure gold (red) and graphene-gold (black) surfaces functionalized with polypyrrole-NTA/Cu^{2+}/b-CT at two different anti-CT concentrations (a, b: 4 ng·$mL^{-1}$and c, d: 35 ng·mL^{-1}). The polymer film was formed under controlled potential electrolysis (0.95 V, 1 mC·cm^{-2}).

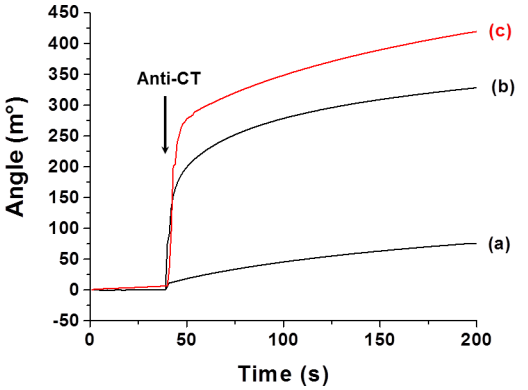

Figure 4. SPR angle change after 35 ng·mL^{-1} of anti-CT injection using polypyrrole-NTA/Cu^{2+}/b-CT on (a) pure gold and (b) graphene-gold. (c) Pyrene-NTA/Cu^{2+}/b-CT graphene-gold surface where the pyrene groups were electropolymerized after formation of an ultrathin layer via π-stacking interactions.

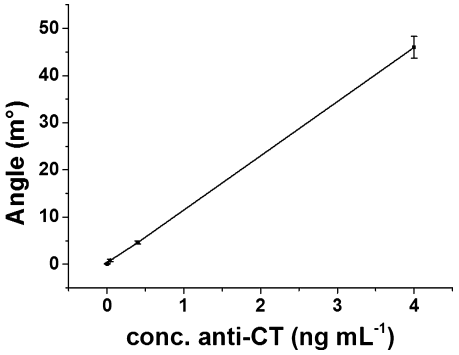

Figure 5. Linear range of the graphene-based SPR immunosensor toward anti-CT.

the antigen receptor. For both surface types, a reflectivity change of around 2% with 35 ng·mL^{-1} of antibody was recorded for the nonspecific binding of the antibody.

One potent method, preserving the unique properties of graphene is noncovalent functionalization with molecules containing an extended π-system, such as pyrene and its derivatives. In order to keep the sensing layer as thin as possible, pyrene-NTA was π-stacked onto graphene giving an ultrathin layer. The successful formation of such a layer was confirmed by XPS measurements, revealing C 1s contributions nearly exclusively from graphene and pyrene-NTA and an estimated thickness of 1.4 nm of the graphene/pyrene-NTA stack, as discussed in the SI. This layer was further stabilized by electropolymerization of the pyrene groups under controlled potential electrolysis via radical coupling at the 3-6 or 3-8 position.[30,31] After identical preparation of the immunosensor as for the polypyrrole-NTA setup, the SPR response was measured in angle change and reflectivity mode. An injection of anti-CT at a concentration of 35 ng·mL^{-1} led to an angle change of 418 mdeg. Compared with the best performing polypyrrole-NTA graphene-gold setup (324 mdeg), the reduced sensing layer thickness improved the SPR immunosensor response by ~80%. This angle shift increase is even more significant when compared with the polypyrrole-NTA setup without graphene (183 mdeg). Here, the angle change increased 150% (Figure 4). These clear improvements can be attributed not only to the SPR signal amplifying properties of graphene but also to the possibility to functionalize graphene with SAM techniques using pyrene derivatives.

Concerning the measurements in reflectivity mode, a 12% increase in reflectivity was recorded with pyrene functionalized graphene-gold SPR immunoensor (Table S1).

The increase is again in the 2-fold range compared to the most optimized polypyrrole setup without graphene. To determine the limit of detection (LOD), the SPR response was recorded for further dilutions of anti-CT in the angle change mode after 50 s. As shown in Figure 5, a linear range could be determined between 0.004 and 4 ng·mL^{-1} (R^2 = 0.9999) with a LOD of 4 pg·mL^{-1} at a relative standard deviation of 9.2% of three identical experiments. Such performances are orders of magnitude higher than comparable electrochemical setups like amperometry,[44] label-free electrochemical impedance spectroscopy,[45] or photoelectrochemical transduction.[46]

Finally, particular care was taken in characterizing nonspecific binding of anti-CT on the functionalized graphene surface. Control experiments were performed under identical conditions by omitting the b-CT immobilization step. In the absence of the antigen receptor unit, a ~2% change in reflectivity and was recorded after injection of 35 ng·mL^{-1} of antibody. This is a non-negligible value for nonspecific binding of the analyte but represents only 20% of the SPR signal intensity. Other control experiments without receptor unit immobilization using polypyrrole-NTA surfaces or untreated graphene-gold were in the same range. Table S1 represents the data of all SPR responses recorded in angle shift, refractive index, and reflectivity mode as well as captured target biomolecules, including control experiments.

In conclusion, the exceptional optical properties of monolayer graphene were exploited to amplify the SPR signals for cholera immunosensing as a disease model. NTA functional groups were attached to CVD grown graphene via electropolymerization of a polypyrrole film or via π-stacking of pyrene derivatives, where this layer was further stabilized by electropolymerization. The NTA anchor group served for the controlled immobilization of the biotinylated bioreceptor cholera toxin. The simple presence of a single graphene sheet increased the SPR sensor performances by 80% compared to the graphene-devoid setup. Furthermore, the best SPR immunosensor was obtained using π-stacking interactions of pyrene-NTA which led to an ultrathin functional layer after electropolymerization.

DOI: 10.1021/ja511512m
J. Am. Chem. Soc. XXXX, XXX, XXX−XXX

The clear advantages of the presence of a monolayer graphene and the possibility of ultrathin functional coatings are most likely extensible to other targets for label free SPR immuno- or DNA sensing.

■ ASSOCIATED CONTENT

Supporting Information

Graphene synthesis, transfer and characterization, materials and methods. This material is available free of charge via the Internet at http://pubs.acs.org.

■ AUTHOR INFORMATION

Corresponding Authors

*serge.cosnier@ujf-grenoble.fr
*michael.holzinger@ujf-grenoble.fr

Notes

The authors declare no competing financial interest.

■ ACKNOWLEDGMENTS

The authors would like to thank the platform 'functionalization of surfaces and transduction' of the scientific structure "Nanobio" for providing facilities and Arielle Le Pellec for assistance. The authors would also like to thank the French−Canadian Research Found (FCRF) for the Ph.D. fellowship for M.S. and the PHC ULYSSES 2012 project no. 27716UF for travel expenses between France and Ireland. The present work was partially supported by the Labex ARCANE (ANR-11-LABX-0003-01). S.W. and G.S.D. thank Science Foundation Ireland under SFI-Pica "GREES" (PI_10/IN.1/I3030) M.T. acknowledges NSERC strategic grant contribution to her SPR-based biosensor research.

■ REFERENCES

(1) Wijaya, E.; Lenaerts, C.; Maricot, S.; Hastanin, J.; Habraken, S.; Vilcot, J.-P.; Boukherroub, R.; Szunerits, S. *Curr. Opin. Solid State Mater. Sci.* **2011**, *15*, 208−224.

(2) Kelly, K. L.; Coronado, E.; Zhao, L. L.; Schatz, G. C. *J. Phys. Chem. B* **2002**, *107*, 668−677.

(3) Guo, X. *J. Biophotonics* **2012**, *5*, 483−501.

(4) Pedersen, D. B.; Duncan, E. J. S. *Technical Report 2005-109*; Defence R&D Canada: Ottawa, Ontario, 2005.

(5) Malic, L.; Sandros, M. G.; Tabrizian, M. *Anal. Chem.* **2011**, *83*, 5222−5229.

(6) Wang, J.; Song, D.; Wang, L.; Zhang, H.; Zhang, H.; Sun, Y. *Sens. Actuators, B* **2011**, *157*, 547−553.

(7) Chaki, N. K.; Vijayamohanan, K. *Biosens. Bioelectron.* **2002**, *17*, 1−12.

(8) Cosnier, S.; Holzinger, M. *Chem. Soc. Rev.* **2011**, *40*, 2146−2156.

(9) Geim, A. K. *Science* **2009**, *324*, 1530−1534.

(10) Geim, A. K.; Novoselov, K. S. *Nat. Mater.* **2007**, *6*, 183−191.

(11) Wang, Y.; Li, Z.; Wang, J.; Li, J.; Lin, Y. *Trends Biotechnol.* **2011**, *29*, 205−212.

(12) Salavagione, H. J.; Diez-Pascual, A. M.; Lazaro, E.; Vera, S.; Gomez-Fatou, M. A. *J. Mater. Chem. A* **2014**, *2*, 14289−14328.

(13) Bonaccorso, F.; Sun, Z.; Hasan, T.; Ferrari, A. C. *Nat. Photonics* **2010**, *4*, 611−622.

(14) Bao, Q.; Loh, K. P. *ACS Nano* **2012**, *6*, 3677−3694.

(15) Nair, R. R.; Blake, P.; Grigorenko, A. N.; Novoselov, K. S.; Booth, T. J.; Stauber, T.; Peres, N. M. R.; Geim, A. K. *Science* **2008**, *320*, 1308−1308.

(16) Wu, L.; Chu, H. S.; Koh, W. S.; Li, E. P. *Opt. Express* **2010**, *18*, 14395−14400.

(17) Bruna, M.; Borini, S. *Appl. Phys. Lett.* **2009**, *94*, 031901.

(18) Jacek, G.; Dawn, T. H. T. *Nanotechnology* **2013**, *24*, 185202.

(19) Song, B.; Li, D.; Qi, W.; Elstner, M.; Fan, C.; Fang, H. *ChemPhysChem* **2010**, *11*, 585−589.

(20) Georgakilas, V.; Otyepka, M.; Bourlinos, A. B.; Chandra, V.; Kim, N.; Kemp, K. C.; Hobza, P.; Zboril, R.; Kim, K. S. *Chem. Rev.* **2012**, *112*, 6156−6214.

(21) Chiu, N.-F.; Huang, T.-Y.; Lai, H.-C.; Liu, K.-C. *Nanoscale Res. Lett.* **2014**, *9*, 1−7.

(22) Wang, L.; Zhu, C.; Han, L.; Jin, L.; Zhou, M.; Dong, S. *Chem. Commun.* **2011**, *47*, 7794−7796.

(23) Zhang, H.; Song, D.; Gao, S.; Zhang, J.; Zhang, H.; Sun, Y. *Sens. Actuators, B* **2013**, *188*, 548−554.

(24) Zhang, J.; Sun, Y.; Xu, B.; Zhang, H.; Gao, Y.; Zhang, H.; Song, D. *Biosens. Bioelectron.* **2013**, *45*, 230−236.

(25) Wirtz, C.; Lee, K.; Hallam, T.; Duesberg, G. S. *Chem. Phys. Lett.* **2014**, *595*−*596*, 192−196.

(26) Choi, S. H.; Kim, Y. L.; Byun, K. M. *Opt. Express* **2011**, *19*, 458−466.

(27) Zagorodko, O.; Spadavecchia, J.; Serrano, A. Y.; Larroulet, I.; Pesquera, A.; Zurutuza, A.; Boukherroub, R.; Szunerits, S. *Anal. Chem.* **2014**, *86*, 11211−11216.

(28) Szunerits, S.; Maalouli, N.; Wijaya, E.; Vilcot, J.-P.; Boukherroub, R. *Anal. Bioanal. Chem.* **2013**, *405*, 1435−1443.

(29) Eigler, S.; Hirsch, A. *Angew. Chem., Int. Ed.* **2014**, *53*, 7720−7738.

(30) Haddad, R.; Holzinger, M.; Villalonga, R.; Neumann, A.; Roots, J.; Maaref, A.; Cosnier, S. *Carbon* **2011**, *49*, 2571−2578.

(31) Waltman, R. J.; Bargon, J. *Can. J. Chem.* **1986**, *64*, 76−95.

(32) Hallam, T.; Berner, N. C.; Yim, C.; Duesberg, G. S. *Adv. Mater. Interfaces* **2014**, *1*, 1400115−1400121.

(33) Peltekis, N.; Kumar, S.; McEvoy, N.; Lee, K.; Weidlich, A.; Duesberg, G. S. *Carbon* **2012**, *50*, 395−403.

(34) Mews, A.; Koberling, F.; Basché, T.; Philipp, G.; Duesberg, G. S.; Roth, S.; Burghard, M. *Adv. Mater.* **2000**, *12*, 1210−1214.

(35) Xu, W.; Xiao, J.; Chen, Y.; Chen, Y.; Ling, X.; Zhang, J. *Adv. Mater.* **2013**, *25*, 928−933.

(36) Kim, N.; Oh, M. K.; Park, S.; Kim, S. K.; Hong, B. H. *Bull. Korean Chem. Soc.* **2010**, *31*, 999−1003.

(37) Wang, Y. Y.; Ni, Z. H.; Shen, Z. X.; Wang, H. M.; Wu, Y. H. *Appl. Phys. Lett.* **2008**, *92*, 043121.

(38) Ferrari, A. C.; Basko, D. M. *Nat. Nano* **2013**, *8*, 235−246.

(39) Wink, T.; J. van Zuilen, S.; Bult, A.; P. van Bennekom, W. *Analyst* **1997**, *122*, 43R−50R.

(40) Ferrari, A. C.; Meyer, J. C.; Scardaci, V.; Casiraghi, C.; Lazzeri, M.; Mauri, F.; Piscanec, S.; Jiang, D.; Novoselov, K. S.; Roth, S.; Geim, A. K. *Phys. Rev. Lett.* **2006**, *97*, 187401.

(41) Sicard, C.; Brennan, J. D. *MRS Bull.* **2013**, *38*, 331−334.

(42) Baur, J.; Holzinger, M.; Gondran, C.; Cosnier, S. *Electrochem. Commun.* **2010**, *12*, 1287−1290.

(43) Stenberg, E.; Persson, B.; Roos, H.; Urbaniczky, C. *J. Colloid Interface Sci.* **1991**, *143*, 513−526.

(44) Ionescu, R. E.; Gondran, C.; Cosnier, S.; Gheber, L. A.; Marks, R. S. *Talanta* **2005**, *66*, 15−20.

(45) Haddour, N.; Chauvin, J.; Gondran, C.; Cosnier, S. *J. Am. Chem. Soc.* **2006**, *128*, 9693−9698.

(46) Yao, W.; Le Goff, A.; Spinelli, N.; Holzinger, M.; Diao, G.-W.; Shan, D.; Defrancq, E.; Cosnier, S. *Biosens. Bioelectron.* **2013**, *42*, 556−562.

DOI: 10.1021/ja511512m
J. Am. Chem. Soc. XXXX, XXX, XXX−XXX